110

SATELLITE & MESOMETEOROLOGY RESEARCH PROJECT

Department of the Geophysical Sciences
The University of Chicago

METRACOM SYSTEM OF CLOUD-VELOCITY DETERMINATION FROM GEOSTATIONARY SATELLITE PICTURES

by

Yun-Mei Chang, Jaime J. Tecson and T. Theodore Fujita

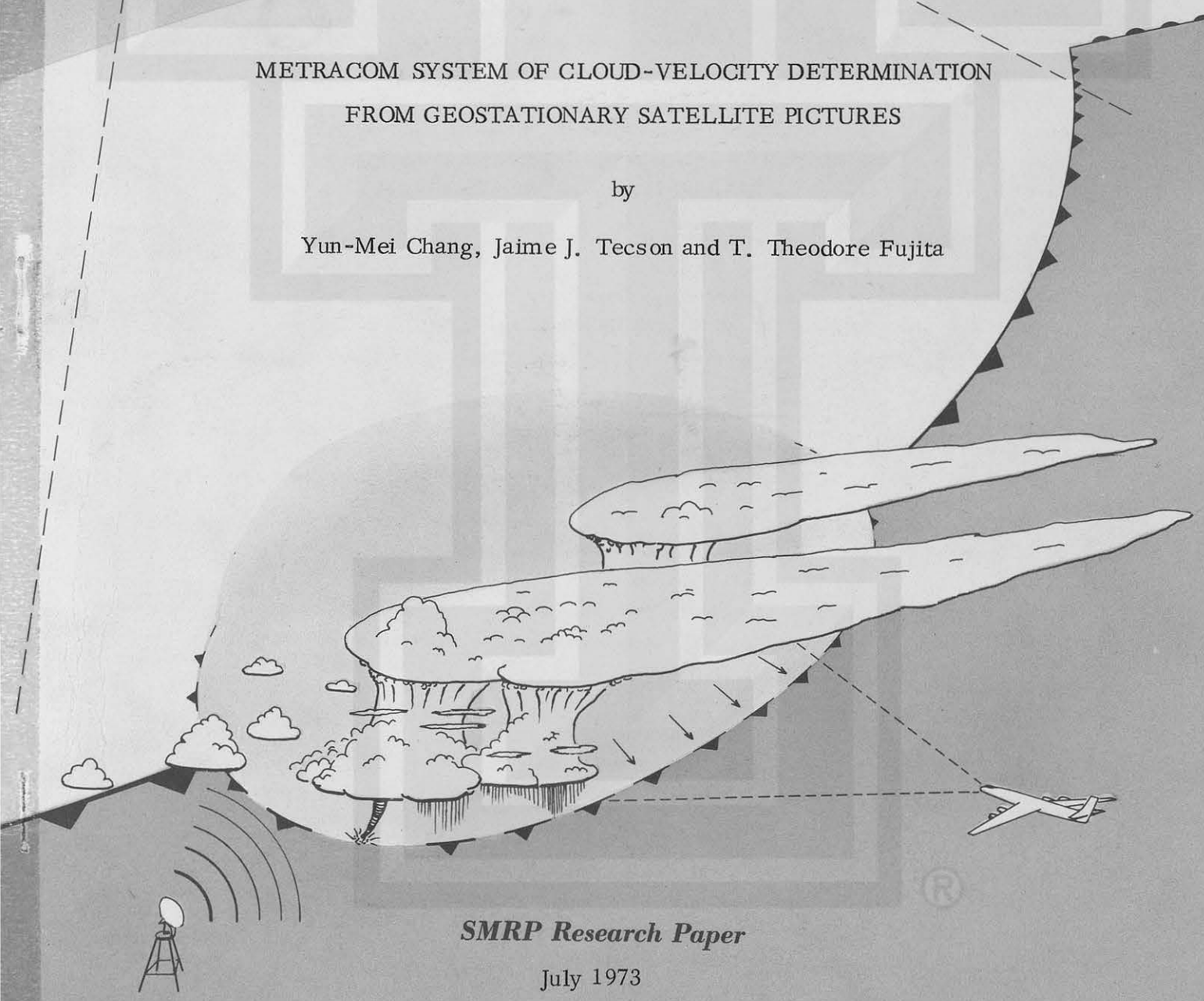

SMRP Research Paper

July 1973

MESOMETEOROLOGY PROJECT --- RESEARCH PAPERS

1.* Report on the Chicago Tornado of March 4, 1961 - Rodger A. Brown and Tetsuya Fujita

2.* Index to the NSSP Surface Network - Tetsuya Fujita

3.* Outline of a Technique for Precise Rectification of Satellite Cloud Photographs - Tetsuya Fujita

4.* Horizontal Structure of Mountain Winds - Henry A. Brown

5.* An Investigation of Developmental Processes of the Wake Depression Through Excess Pressure Analysis of Nocturnal Showers - Joseph L. Goldman

6.* Precipitation in the 1960 Flagstaff Mesometeorological Network - Kenneth A. Styber

7.** On a Method of Single- and Dual-Image Photogrammetry of Panoramic Aerial Photographs - Tetsuya Fujita

8. A Review of Researches on Analytical Mesometeorology - Tetsuya Fujita

9.* Meteorological Interpretations of Convective Nephsystems Appearing in TIROS Cloud Photographs - Tetsuya Fujita, Toshimitsu Ushijima, William A. Hass, and George T. Dellert, Jr.

10.* Study of the Development of Prefrontal Squall-Systems Using NSSP Network Data - Joseph L. Goldman

11. Analysis of Selected Aircraft Data from NSSP Operation, 1962 - Tetsuya Fujita

12. Study of a Long Condensation Trail Photographed by TIROS I - Toshimitsu Ushijima

13. A Technique for Precise Analysis of Satellite Data; Volume I - Photogrammetry (Published as MSL Report No. 14) - Tetsuya Fujita

14. Investigation of a Summer Jet Stream Using TIROS and Aerological Data - Kozo Ninomiya

15. Outline of a Theory and Examples for Precise Analysis of Satellite Radiation Data - Tetsuya Fujita

16. Preliminary Result of Analysis of the Cumulonimbus Cloud of April 21, 1961 - Tetsuya Fujita and James Arnold

17. A Technique for Precise Analysis of Satellite Photographs - Tetsuya Fujita

18.* Evaluation of Limb Darkening from TIROS III Radiation Data - S.H.H. Larsen, Tetsuya Fujita, and W.L. Fletcher

19. Synoptic Interpretation of TIROS III Measurements of Infrared Radiation - Finn Pedersen and Tetsuya Fujita

20.* TIROS III Measurements of Terrestrial Radiation and Reflected and Scattered Solar Radiation - S.H.H. Larsen, Tetsuya Fujita, and W.L. Fletcher

21. On the Low-level Structure of a Squall Line - Henry A. Brown

22.* Thunderstorms and the Low-level Jet - William D. Bonner

23.* The Mesoanalysis of an Organized Convective System - Henry A. Brown

24. Preliminary Radar and Photogrammetric Study of the Illinois Tornadoes of April 17 and 22, 1963 - Joseph L. Goldman and Tetsuya Fujita

25. Use of TIROS Pictures for Studies of the Internal Structure of Tropical Storms - Tetsuya Fujita with Rectified Pictures from TIROS I Orbit 125, R/O 128 - Toshimitsu Ushijima

26. An Experiment in the Determination of Geostrophic and Isallobaric Winds from NSSP Pressure Data - William Bonner

27. Proposed Mechanism of Hook Echo Formation - Tetsuya Fujita with a Preliminary Mesosynoptic Analysis of Tornado Cyclone Case of May 26, 1963 - Tetsuya Fujita and Robbi Stuhmer

28. The Decaying Stage of Hurricane Anna of July 1961 as Portrayed by TIROS Cloud Photographs and Infrared Radiation from the Top of the Storm - Tetsuya Fujita and James Arnold

29. A Technique for Precise Analysis of Satellite Data, Volume II - Radiation Analysis, Section 6. Fixed-Position Scanning - Tetsuya Fujita

30. Evaluation of Errors in the Graphical Rectification of Satellite Photographs - Tetsuya Fujita

31. Tables of Scan Nadir and Horizontal Angles - William D. Bonner

32. A Simplified Grid Technique for Determining Scan Lines Generated by the TIROS Scanning Radiometer - James E. Arnold

33. A Study of Cumulus Clouds over the Flagstaff Research Network with the Use of U-2 Photographs - Dorothy L. Bradbury and Tetsuya Fujita

34. The Scanning Printer and Its Application to Detailed Analysis of Satellite Radiation Data - Tetsuya Fujita

35. Synoptic Study of Cold Air Outbreak over the Mediterranean using Satellite Photographs and Radiation Data - Aasmund Rabbe and Tetsuya Fujita

36. Accurate Calibration of Doppler Winds for their use in the Computation of Mesoscale Wind Fields - Tetsuya Fujita

37. Proposed Operation of Intrumented Aircraft for Research on Moisture Fronts and Wake Depressions - Tetsuya Fujita and Dorothy L. Bradbury

38. Statistical and Kinematical Properties of the Low-level Jet Stream - William D. Bonner

39. The Illinois Tornadoes of 17 and 22 April 1963 - Joseph L. Goldman

40. Resolution of the Nimbus High Resolution Infrared Radiometer - Tetsuya Fujita and William R. Bandeen

41. On the Determination of the Exchange Coefficients in Convective Clouds - Rodger A. Brown

* Out of Print
** To be published

(Continued on back cover)

METRACOM SYSTEM OF CLOUD-VELOCITY DETERMINATION FROM GEOSTATIONARY SATELLITE PICTURES

by

Yun-Mei Chang, Jaime J. Tecson and T. Theodore Fujita
Department of the Geophysical Sciences
The University of Chicago

SMRP Research Paper No. 110
July 1973

The research reported in this paper was sponsored by the National Oceanic and Atmospheric Administration, NESS, under grant E-198-68 (G) and the National Science Foundation under grant GA 31589.

METRACOM System of Cloud-Velocity Determination From Geostationary Satellite Pictures

by

Yun-Mei Chang, Jaime J. Tecson and T. Theodore Fujita
Department of the Geophysical Sciences
The University of Chicago

ABSTRACT

A system of cloud-velocity determination from sequences of ATS pictures has been developed. Clouds on the time-lapse movie made for computation purposes are tracked by trained meteorologists. Such a tracking will definitely increase the number of trackable clouds in multiple layers. Cloud-motion vectors on the image coordinates are digitized to compute velocities relative to the earth. To compensate for satellite movements around the nominal location and spin axes, the following parameters are included in computations: they are subsatellite latitude and longitude, equatorial and polar diameters, yaw, eccentricity, and skew angle.

The cloud-velocity, thus computed, is called the METRACOM velocity which stands for the cloud velocity TRAcked by METeorologists and computed by COMputer.

Test analyses of cloud velocities were made for a 4-day period of Hurricane Ginger of September, 1971. Results are found to be very useful in the determination of in- and out-flow fields.

1. INTRODUCTION

Since ATS pictures became available to meteorologists in 1966, various attempts have been made to determine velocities of clouds seen in successive pictures. Although cloud displacements can be observed in such picture sequences, the determination of an exact motion vector is essential when a high degree accuracy of the computed velocity is required.

To obtain exact displacement vectors, various groups devised their own methods. At Stanford Research Institute, Serebreny, Evans, Hadfield and Wiegman (1967) developed a method of tracking clouds on a TV image. Original gridded ATS pictures on film were scanned and stored in analog form on magnetic tape and later projected on a TV screen. Motions of individual cells, frontal cloud bands and cirrus could readily be determined. Meanwhile, Fujita, Bradbury, Murino and Hall (1968) used a "Cine-grammetric Method" whereby gridded ATS pictures are made into time-lapse movies. Keeping the cloud velocity computation scheme under constant review, Fujita (1969) has reported on the effects of satellite motion and corrections required on apparent cloud speed and direction. In a report from the Space Science and Engineering Center, The University of Wisconsin (1972), a technique called McIDAS has been developed by Suomi and his group for measuring cloud motion vectors from ATS images displayed on a TV screen using original digital data and computer cross correlation schemes. The advantage of this technique is speed in obtaining results.

The METRACOM system described in this paper is a combination of cloud tracking by trained meteorologists and subsequent calculation of cloud velocity by a computer. The system utilizes a movie loop of a set of picture sequences projected on a screen in front of a trained meteorologist. Clouds to be tracked are selected by the meteorologist while watching the entire field of cloud motion. Each time when he determines the beginning and the end points of the cloud vectors, the cloud-motion vectors are drawn on the movie screen, so that the overall motion field can be recognized more clearly as the tracking goes on.

When the cloud-motion field is mapped as much as possible, it is necessary to determine the coordinates of beginning and end points of each motion vector. To accomplish the computation, a digitizer is used. All the points are converted to digital form so that they eventually become the input data for a computer program to compute the individual cloud velocities.

This system will insure correct tracking of cloud motions and the quick computing of the cloud velocities. This combination of human judgment and computer capability will result in the determination of cloud velocity in meso- or even smaller scale of any area of specific interest.

The flow diagram of METRACOM system is shown in Figure 1.

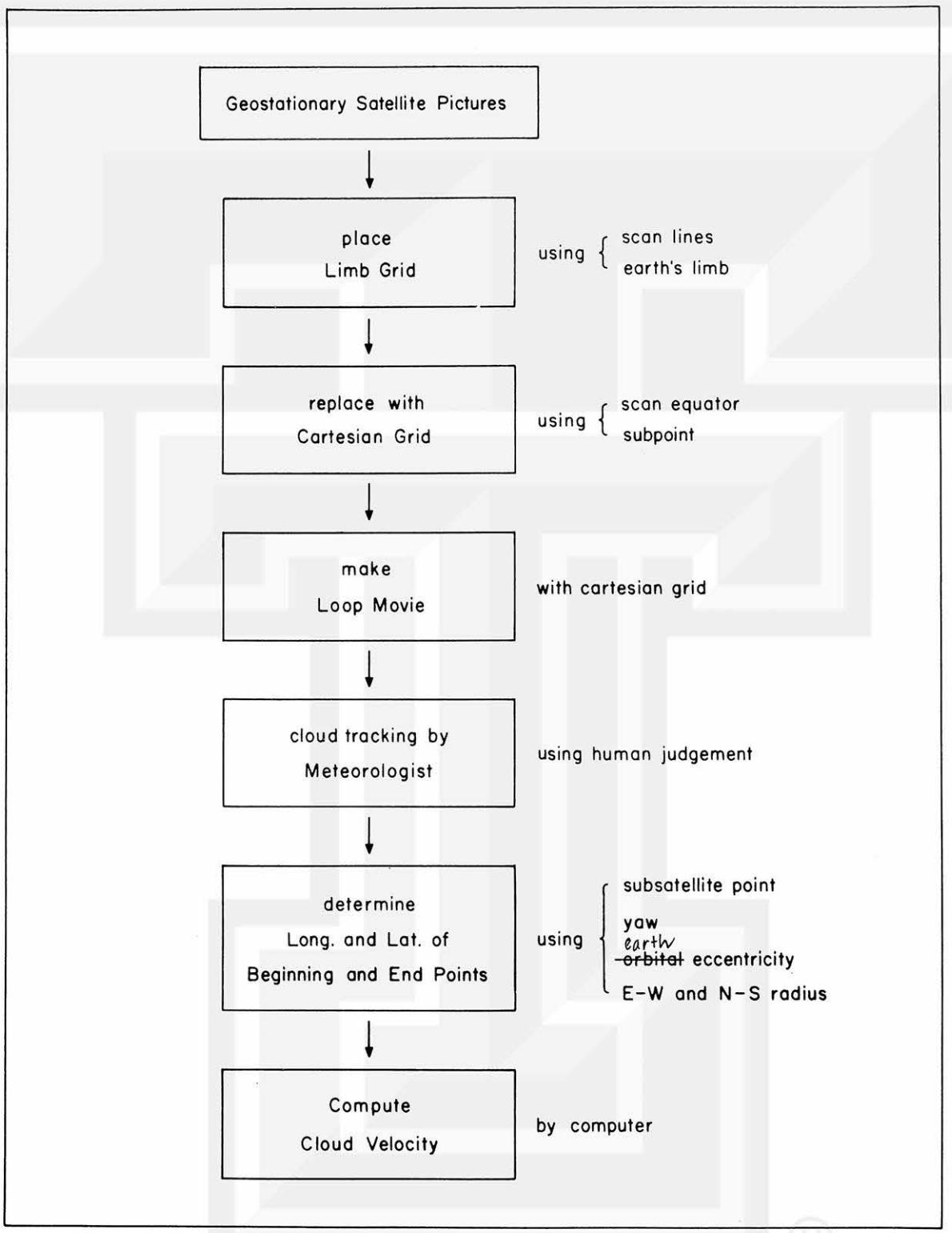

Fig. 1. Flow diagram of the METRACOM System.

2. REGISTRATION

For photographs to be usable for cloud-motion determination, the initial step requires that a reference frame be fixed consistently for each picture that will comprise the series. Otherwise, a systematic error in the final computed vector is introduced. This frame is established by the use of a Limb Grid which, in effect, is a transparent master sheet or foil containing the shape of the full earth's disc with the size that fits those in the photographs, the earth's scan equator including additional lines parallel to it and an almost vertical line symmetric with the earth's east-west configuration.

The choice of the sequence of pictures to be used depends on the following conditions: the best set of consecutive photographs with the most recogniziable disc, of uniformly good photographic quality, with a minimum or absence of "noise" or missynchronization effects and with a period coverage of approximately one hour which is long enough to track most clouds and to derive representative wind vectors.

The ATS pictures are used. In order to know the exact geographical position of any object in the image, the geometric center of the globe image, or the subsatellite point, has first to be determined. This is accomplished by the registration procedure which mainly uses the image horizon and the scan lines on the photographs for alignment. However, since only the sunlit portion of the earth is photographed at intervals during the course of one day, very few pictures would show the entire view of the globe. As should be expected, many of them (Fig. 2) only show part or even less than a half of the globe, while others have only the upper half portion of the earth. For full usage of these photographs, a master Limb Grid has to be used. To devise this grid, one picture which had the most coverage of the globe was selected and its horizon traced as the master since not only the north-south and east-west radii of the image do not vary very much from one photograph to another, but, also, the change of the east-west diameter is linear proportional to the distance between the outer edges of the two upper reference fiducial line segments which appear on the photograph (see Fig. 3). The latter is expressed by the equation

$$x_F = k D_E \tag{1}$$

where D_E is the east-west diameter of the image, x_F is the fiducial distance, that is, the distance between the outer edges of the two upper fiducial marks, and k is the proportionality constant. The master globe or Limb Grid can be photographically

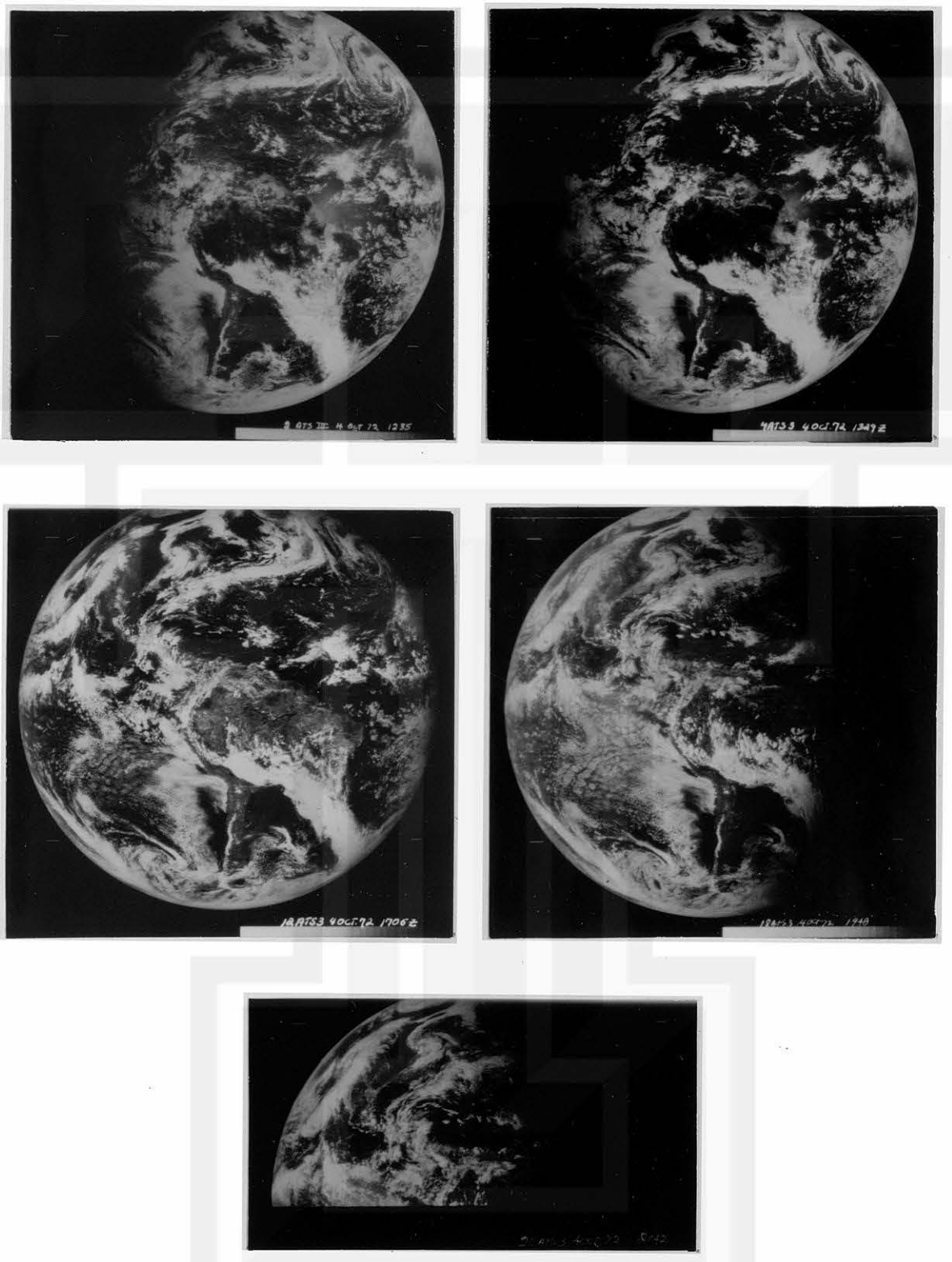

Fig. 2. A sampling of ATS III satellite pictures taken during one day.

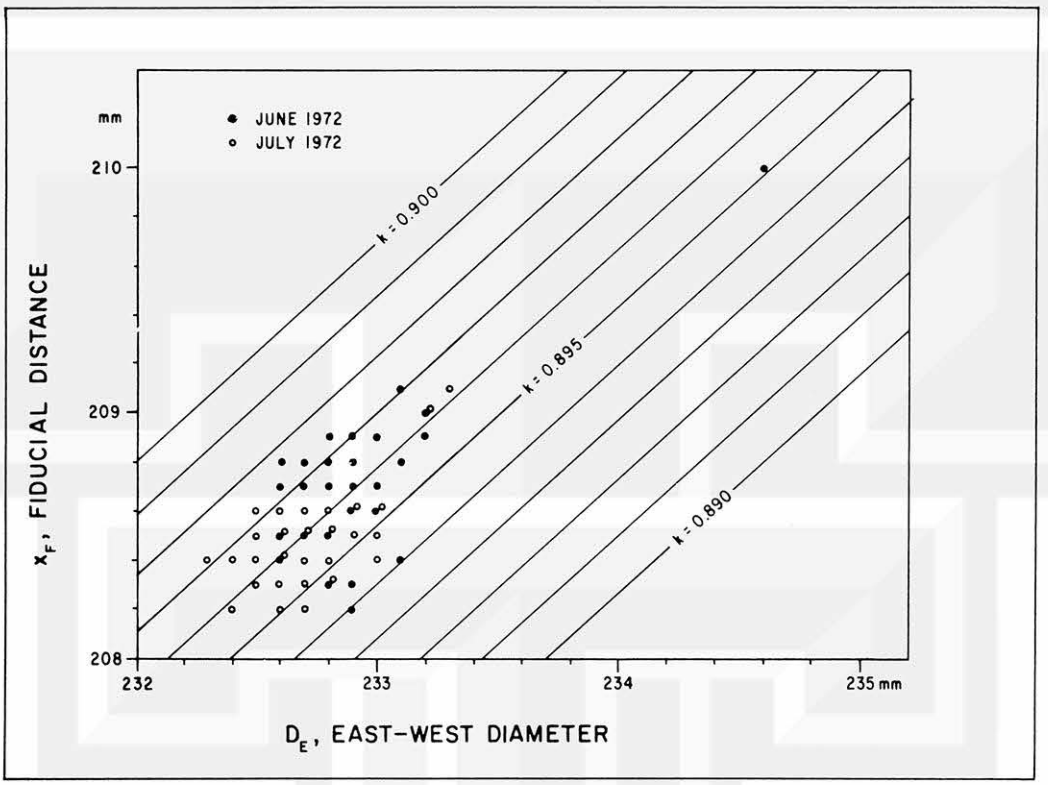

Fig. 3. The variation of east-west diameter (D_E) of the earth image with respect to the fiducial distance (x_F), the distance between the outer edges of the two upper reference fiducial line segments, for June (•) and July (∘), 1972, from NOAA pictures. The straight lines are the lines that fit the equation $x_F = k D_E$ for different proportionality constant k.

enlarged or reduced such that its east-west diameter will be equal to that of the earth's image on the photograph, which can be calculated by knowing the x_F of the photograph.

On the master, a few scan lines with arbitrary intervals are drawn parallel to the two upper fiducial marks. The locus of points bisecting the earth's disc at each scan line is drawn as a straight line and is denoted as the B-axis for the master Limb Grid. This B-axis, which incidentally is the image of the satellite spin axis, is tilted with a small angle, ϵ, clockwise from north. A scan line drawn passing through the center point of the B-axis between its two intersections with the earth's disc in the master grid is the scan equator. This scan equator is taken as the A-axis and its intersection with the B-axis, which is the center of the picture, is taken as the origin of the master

grid. This grid is called the Limb Grid, and the limb can be expressed by the following equation:

$$\frac{(A + B \sin \epsilon)^2}{A_E^2} + \frac{(B \cos \epsilon)^2}{B_N^2} = 1 \qquad (2)$$

where A_E and B_N are the radii along the A-axis (scan equator) and B-axis (satellite spin axis), respectively.

For any photograph to be used in the series, a Limb Grid of appropriate size is superimposed and attached in such a manner that the picture horizon fits the Limb Grid horizon and also that any scan line of the picture is parallel to the scan equator of the Limb Grid. Noting that the change of the skew angle (ϵ) in the image is so small that it can be considered negligible, we take ϵ as a constant. Any point image on the picture can then be expressed by this Limb Grid.

3. MOVIE WITH CARTESIAN GRID

Eventually, a movie loop is required to produce motion from the sequence of photographs which are now aligned by a Limb Grid attached to each picture. In preparation for this, this series has to be permanently registered to insure and correct motion of the systems and the clouds surrounding them. This is achieved to a high degree of precision by the use of a Punch Board (Fig. 4) where holes are punched on each photograph for alignment purposes after each attached Limb Grid coincides with an identical grid held fixed with the Punch Board. After registering the photographs, a transparent Cartesian Grid is taped on each picture. This is done by setting the x-axis and the origin point of the Cartesian Grid coincident, respectively, with the scan equator, or A-axis, and its intersection point with the B-axis of the Limb Grid. The Limb Grid is then removed. The Cartesian Grid and the coordinates shown on the picture are called the picture grid and picture coordinates, respectively.

Thereafter, a movie loop is prepared using an Animation Camera (Fig. 5) by exposing each photograph, arranged in sequence, a fixed number of times. More specifically, this is done by allowing more exposure frames (say 30) for the first photograph, followed by lesser number of exposure frames (say 3) for the rest, except the last photograph which again is exposed more (say 30). Experience has shown that the tracing of cloud elements is made easier if, after filming the forward motion of the clouds as detailed above, the backward motion, or retrace, follows immediately. This is accomplished by exposing an

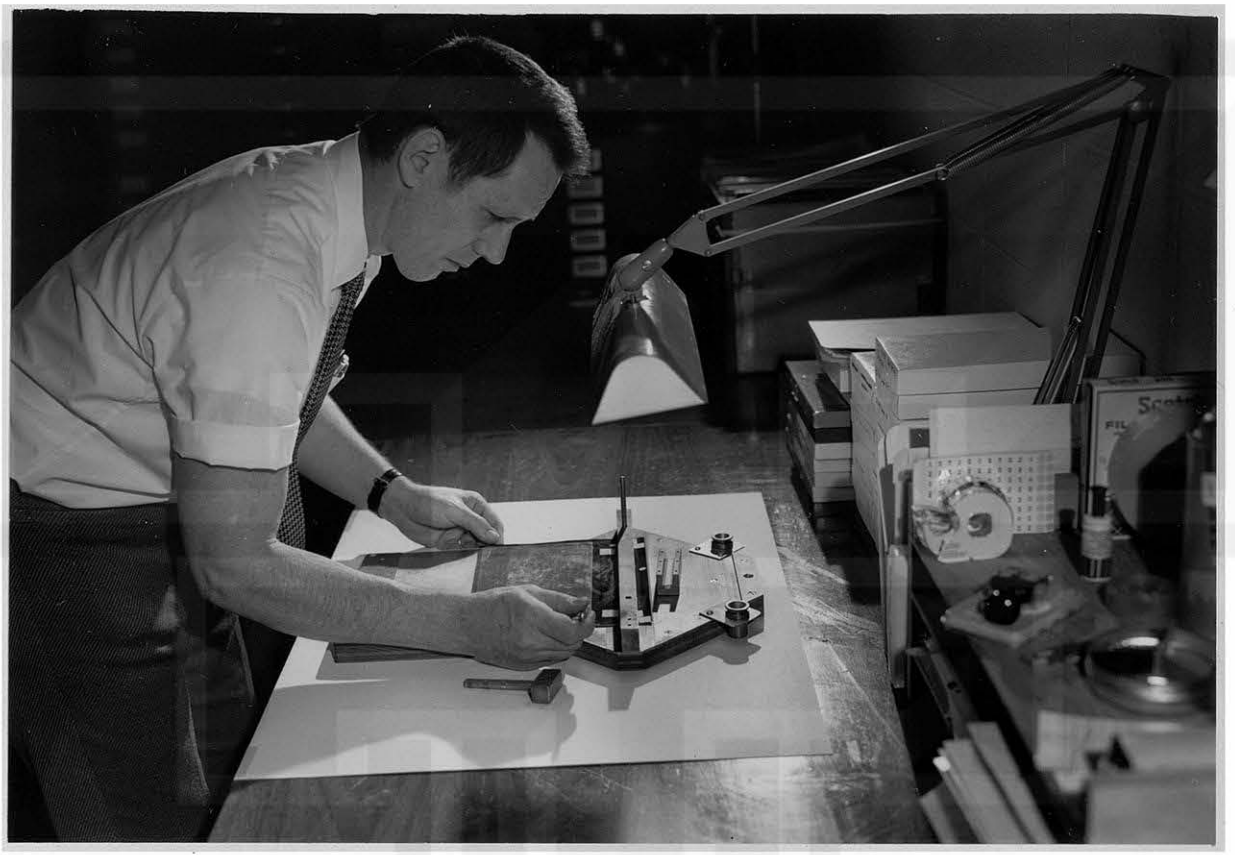

Fig. 4. A Punch Board for use in registering the sequence of ATS pictures prior to being photographed into a movie loop.

even lesser number of frames (say 1), this time in reverse order or sequence, the pictures next preceding the last, and the rest, up to the second picture. The whole procedure constitutes what is termed a film cycle and may be repeated any number of times to suit the length of the movie loop desired. Assuming a hypothetical series consisting of n photographs, numbered in sequence according to increasing time, one such cycle of the movie loop is illustrated below.

Picture Number	1	2	...	n-1	n	n-1	...	3	2
Number of Exposures	30	3	...	3	30	1	...	1	1

To determine the limb coordinate (A,B) for any point image with picture coordinate (x,y), the north-south radius (B_N) of the earth's image on the picture is taken as a constant, that is, the north-south radius of the master Limb Grid before it is photographically enlarged or reduced, since the change of B_N is so small that it can be neglected. Then, if we choose 1000 as the unit of the radius of the globe, any point P with the

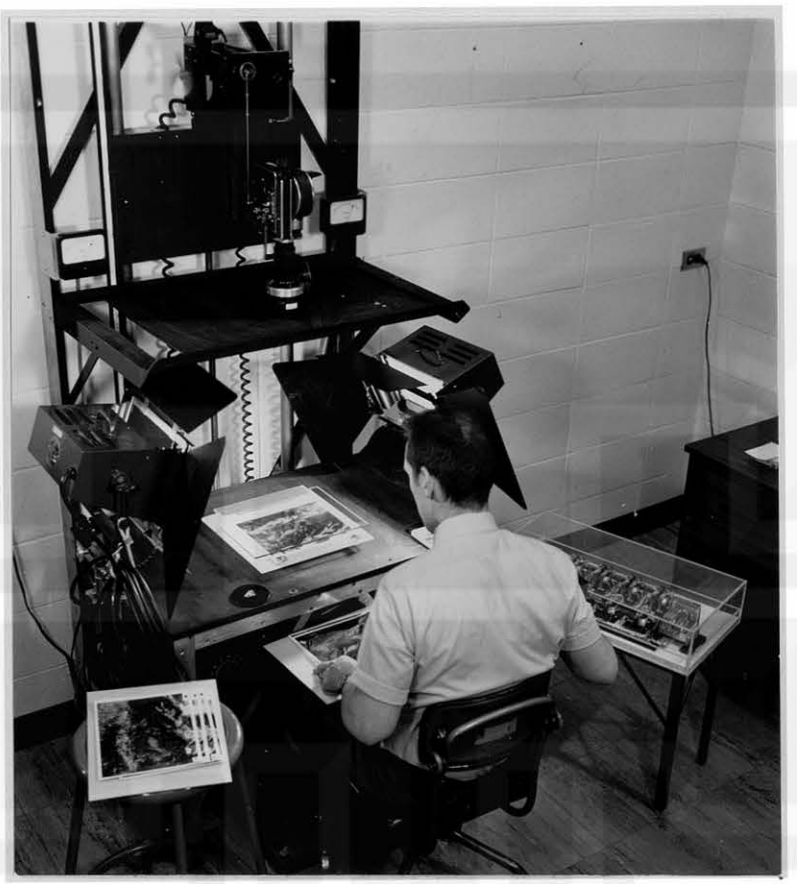

Fig. 5. An Animation Camera system capable of various magnifications (Zoom effect) of desired areas and with precise control of frame exposure count for each of the ATS pictures to be photographed into a movie loop.

picture coordinate (x,y) on the image can be transferred to the Limb Grid coordinate (A,B) by:

$$A = (x_p - y_p \tan \epsilon) \frac{1000}{x_E} \qquad (3)$$

$$B = (y_p \sec \epsilon) \frac{1000}{y_N \csc \epsilon} \qquad (4)$$

where $x_E = \frac{1}{2} D_E$, since D_E can be calculated from Eq. (1), y_N is the projection of the north-south radius of the earth's image on the y-axis (which is taken as a constant), and subscript | p refers to any point on the image, while ϵ is the skew angle of the Limb Grid as discussed in Section 2 (see Fig. 6). Hence, the transformation between (x,y) and (A,B) coordinates involves a rotation in the B-axis (tan ϵ in Eq. (3)) and an amplification factor between the two coordinates, namely, $1000/x_E$ in Eq. (3) and $1000/y_N \csc \epsilon$ in Eq. (4),

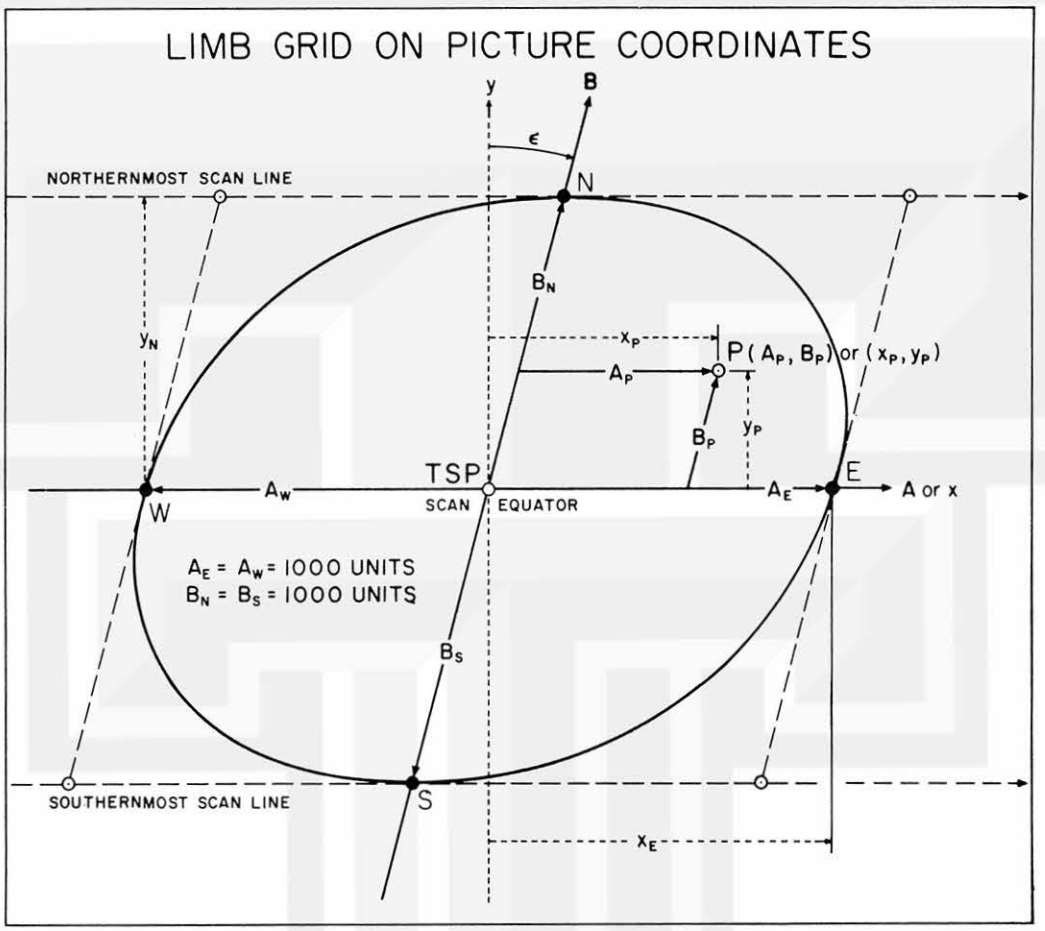

Fig. 6. Limb Grid (A, B) with picture coordinate (x, y). The ellipse stands for the limb of the image. ϵ is the skew angle. A_E and B_N are the east-west and north-south radii of the limb of the earth disc, respectively.

since, in the picture grid, x_E and $y_N \cdot \csc \epsilon$ correspond to A = 1000 and B = 1000 on the Limb Grid, respectively, and these two grids have the same origin.

4. TRACKING BY METEOROLOGIST

With the movie loop completed, it is then projected by a specially designed and constructed Loop Projector (Fig. 7) onto a rectangular plate glass which also serves as a tracing surface. Tracing of the motion of the elements in the movie loop is done directly on a sheet of tracing paper placed on the outer surface of this glass. In addition to the cloud vectors which are plotted, motions of as many discernible known landmarks are tracked and all grid points are traced. It will appear that the picture grid points are distorted due to optical effects.

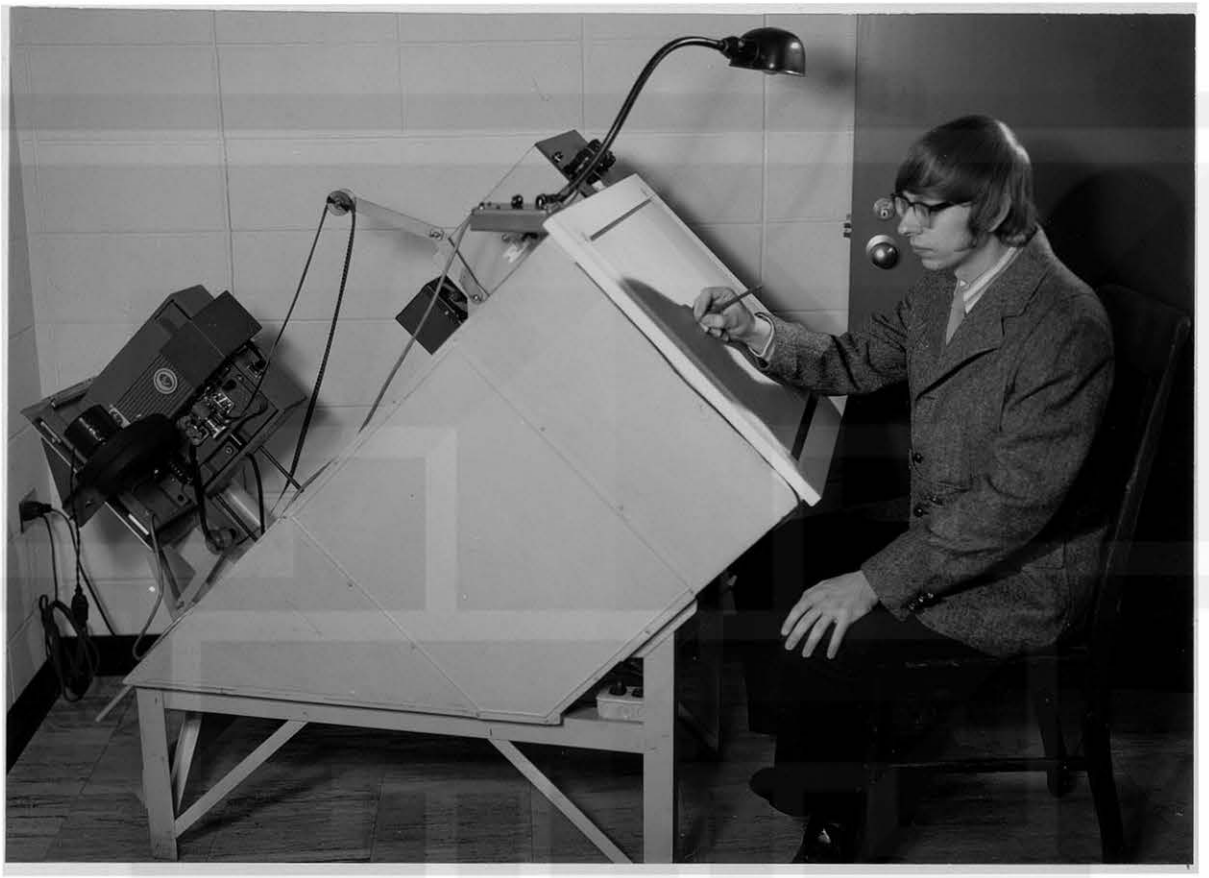

Fig. 7. A Movie Loop Projector for use in tracing motions of cloud elements directly on an opaque glass plate screen.

At first thought, it may seem a bit incongruous that meteorologists are preferred to perform the monotonously mechanical chore of tracking motion and drawing vectors when equally capable technical personnel could do the task. Tracing elements from a movie loop is not as simple as it would sound or as it would appear to be. A good amount of judgment is required and meteorological know-how dictates such judgment. Although in the final analysis it is only the cloud vector that is evaluated, the tracking process may turn out to be confusing at times. In the first place, distinction should be made as to whether or not the element being traced is a cloud, landmark or terrain. A knowledge of the general flow pattern of the system under study aside from its translatory motion, as in hurricanes, becomes very helpful in making certain that vector directions as correctly labeled. There should be an awareness that differences in the overall flow pattern are likely to be encountered due mainly to cloud motions at various levels. Familiarity with the appearance and configurations of general types of high, middle and low clouds becomes a valuable aid in this respect. Flow patterns induced by land- or sea-breeze effect near

or over coastal areas should be kept in mind. Care should be taken such that only clouds that persist during the whole period of the loop are traced. Otherwise, vector magnitudes are seriously misrepresented. Decaying as well as developing clouds should therefore be carefully observed. Altogether, these factors require the selective ability to generate the maximum number of compatible and usable data in the area under study, a particular task that only a meteorologist can capably perform.

5. DIGITIZER TECHNIQUE FOR COORDINATE TRANSFORMATION

The tracing paper becomes the worksheet for cloud velocity computations after the motion of all recognizable cloud elements and landmarks have been traced onto it from the movie loop projection. These velocity vectors have to be evaluated then. One approach would be to resolve each into components using some coordinate system which then becomes input data to a computational scheme.

A simple, efficient, accurate and fast method employed is through the use of an electronic digitizer system -- a high-precision, X-Y coordinate measuring unit that converts graphical data into digital form for computer applications (see Fig. 8).

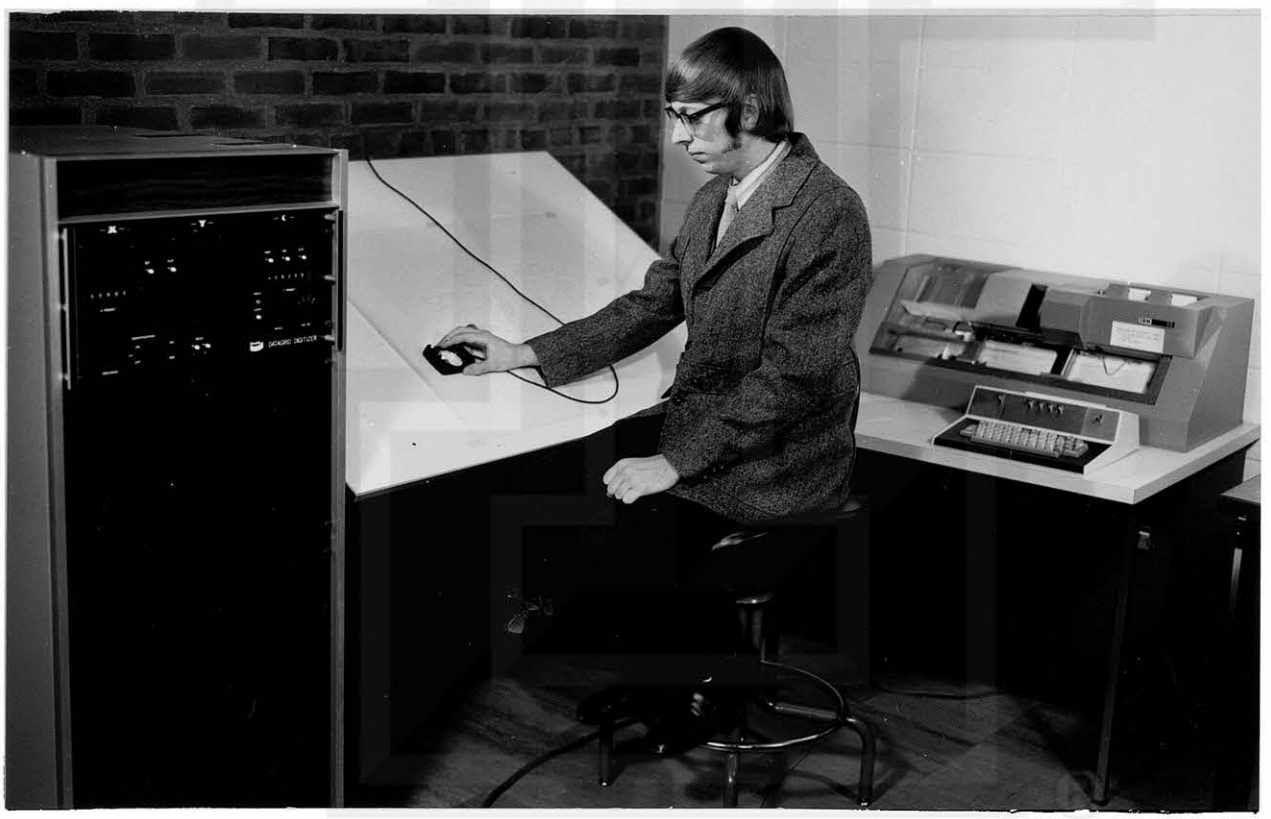

Fig. 8. An electronic digitizing equipment consisting of a working surface or digitizing area, a free-moving cursor, a display and control panel linked to a card punch output machine for X- and Y-axis readout (resolution 0.001 inch and accuracy ± 0.005 inch) of cloud vectors for direct computer processing.

Direct readouts of the X and Y coordinates of the beginning and end points of each vector are punched into a data card.

In order to establish the X-Y coordinates on the digitizer board, it is necessary to select a point at which digitizer registers X = 0 and Y = 0. This point called the "digitizer origin" is selected as being one of the grid points near the image center on the board.

As shown in Fig. 9, grid lines are distorted due mainly to the optics of both camera and projector. The vector connecting a grid point on the tracing paper with its undistorted position is called the distortion vector. We will have to expect that distortion exists everywhere. For convenience, however, we assume that the distortion at the pre-selected origin (X = 0, Y = 0) is zero, so that the distortion under consideration is the relative distortion rather than the absolute one.

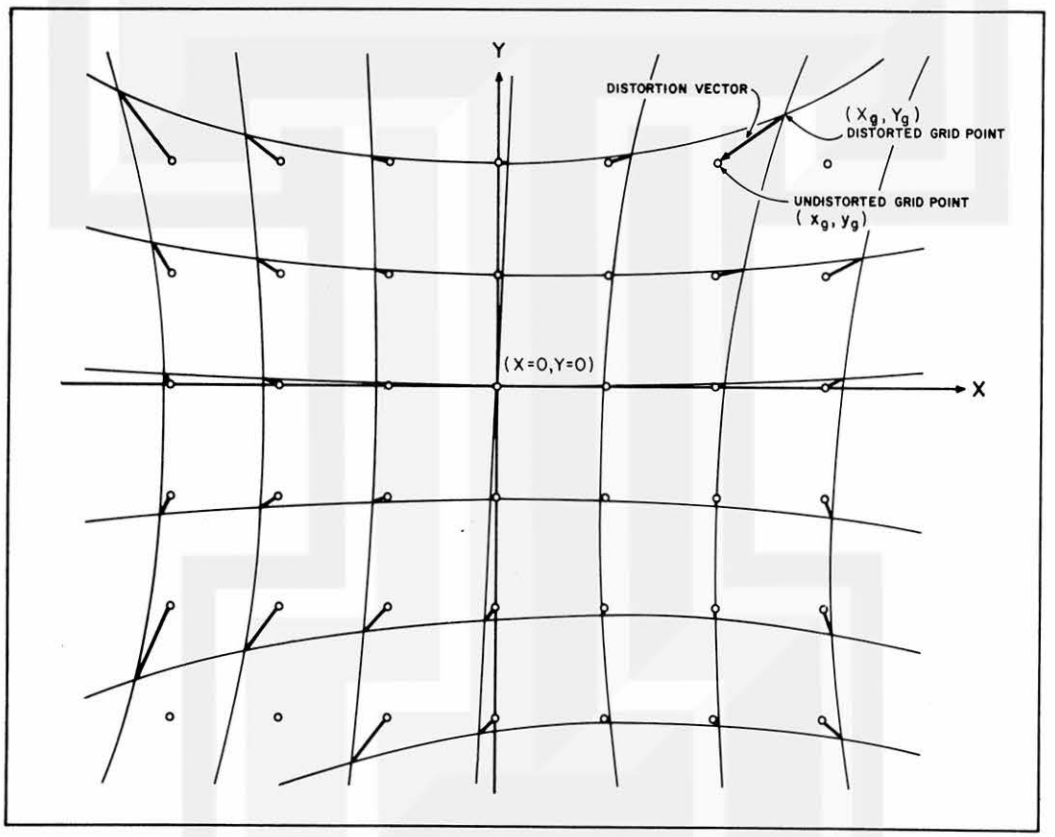

Fig. 9. An image of the Cartesian Grid placed on the digitizer board. The grid lines are distorted due to the optics of camera and projector. Small open circles denote the grid positions which would appear if there were no distortions. A correction vector is applied to each grid point.

In order to minimize the relative distortion within the image, dimensions of the outermost grid points are used to compute the scale factors, f_x in the x direction and f_y in the y direction. In most cases f_x is very close to f_y.

Expressing the x and y components of the error vector at a point P on the digitizer board, by Δx and Δy, respectively, we write transformation equations as:

$$x_p = (x_o + X_p f_x) + \Delta x_p \qquad (5)$$

$$y_p = (y_o + Y_p f_y) + \Delta y_p \qquad (6)$$

where x_p and y_p denote the Cartesian coordinates of the point P. X_p and Y_p are the coordinates of P measured by the digitizer. Since a Cartesian Grid point is selected as the digitizer origin, x_o and y_o are expressed by integers such as 1.000, 2.000, ... etc.

To calculate the correction factors Δx and Δy, all the grid points on the movie are also digitized as (X_g's , Y_g's) . Suppose (x_g, y_g) is the grid point coordinate which is known in the picture grid (see Fig. 9), then, following equation (5) and (6), the correction factors for grid point G can be calculated by

$$\Delta x_g = x_g - (x_o + X_g f_x) \qquad (7)$$

$$\Delta y_g = y_g - (y_o + Y_g f_y) \qquad (8)$$

where the subscript "g" refers to grid point G in the picture grid.

For this study, Δx_g's and Δy_g's for all the grid points in the picture grid are found to be very small and are less than one-hundredth of a picture coordinate unit, so the correction factors $(\Delta x_p, \Delta y_p)$ for point P can be obtained by simply taking the linear interpolation of the error field of the four grid points which surround the point P. Hence, equations (5) and (6) are used after equations (7) and (8) are solved.

6. LOCAL ENLARGEMENT PICTURES

For more accurate results, local enlargement photographs are used. These are obtained by simply enlarging certain areas of interest in the global pictures.

An identified landmark is selected as reference point, both for the global pictures, and the enlargement pictures. A Cartesian Grid is attached on each enlargement picture in such a way that the x-axis is parallel to the scan line with the landmark at the origin

point. Hence, following the procedure described above (Section 3), a movie loop is made with the enlargement pictures. Here, the landmark does not move. Then the cloud motion can be traced from a loop projector and digitized into digital data as discussed in the former chapters (Section 4, 5).

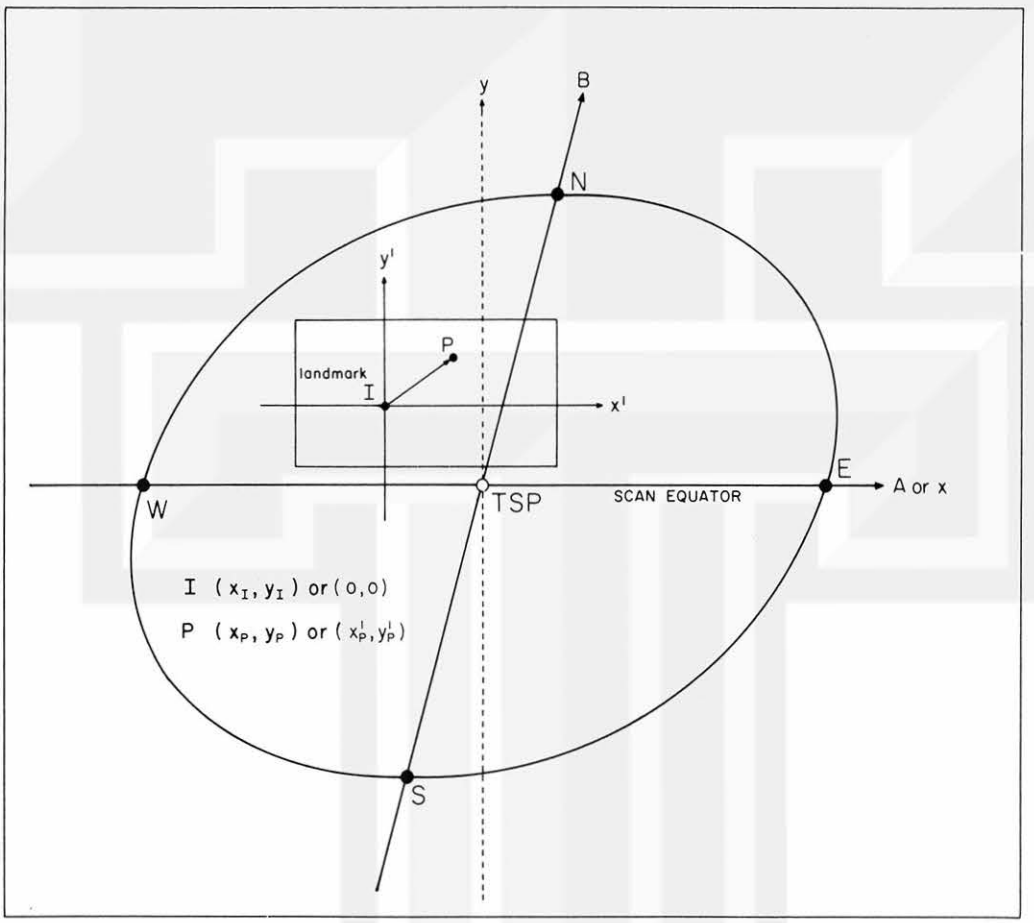

Fig. 10. Local enlargement from global picture. The area bounded by thin line is the local area which is going to be enlarged. Point I is the landmark which is fixed on the movie loop and point P is any cloud object.

To transform the movie coordinate (X, Y) to the picture coordinate (x, y) as defined in Section 5, scale factors F_x , F_y , in x and y directions, respectively, and the location of the fixed landmark in global pictures are required. The scale factors, F_x , F_y , are determined by the ratio of the global picture size and the enlargement picture size. As shown in Fig. 10, point I is the fixed landmark with the picture coordinate (x_I, y_I), then following equation (5) and (6) the picture coordinate for the object point p can be obtained by the following formulas

$$x_p = x_I + \left[(x_o' + X_p \, f_{x'}) + \Delta x_p' \right] \cdot F_x \qquad (9)$$

$$y_p = y_I + \left[(y_o' + Y_p \, f_{y'}) + \Delta y_p' \right] \cdot F_y \qquad (10)$$

where "'" indicates the coordinate which is read off from the local enlargement pictures and where x_o', y_o', X_p, Y_p, $f_{x'}$, $f_{y'}$, $\Delta x_p'$, $\Delta y_p'$ are defined in the enlargement pictures in the same manner as x_o, y_o, X_p, Y_p, f_x, f_y, Δx_p, Δy_p are defined in the global pictures in Chapter 5.

Motions of clouds are traced from movie loop made by those local enlarged satellite pictures. Much more cloud elements can be traced easily and cloud motions can be distinguished clearly than by using the global pictures. It does give much accurate results in determining the in- and out-flow patterns.

7. CLOUD-VELOCITY COMPUTATION

The movement of clouds shown from the movie on the loop projector gives the general pattern and intensity of flow around the area under investigation. However, because of the spherical geometry relating the earth with the satellite and the motion of the satellite, the geometrical relations between the image on the picture and the exact geographical position on the earth have to be resolved. Hence, it is necessary to transform the cloud vectors from Limb Coordinate (A,B) to the geographic earth coordinate, namely, latitude (ϕ) and longitude (θ). The position of the subsatellite point (ϕ_s, θ_s) and the inclination of the satellite spin axis (w) are necessary input for this transformation (see Appendix C for the determination of ϕ_s, θ_s and w). After the cloud vectors are digitized into digital format and finally transformed to picture coordinates (x,y) as discussed in Section 5, these digital data, as well as the already determined parameters (ϕ_s, θ_s, w) will be the input for computer processing. A flow chart (Fig. 11) outlining the procedures for the determination of the geographical coordinate follows (see Appendix B for the determination of ϕ and θ).

The cloud velocity can then be calculated by knowing the exact geographical position of the beginning and end points of all the cloud vectors traced from the loop projector, and also, by knowing the exact time of the beginning and end frames of the ATS photographs from which the movie was made. The cloud velocity is the vectorial arc on the great circle passing through the beginning and end points of the vector divided by the

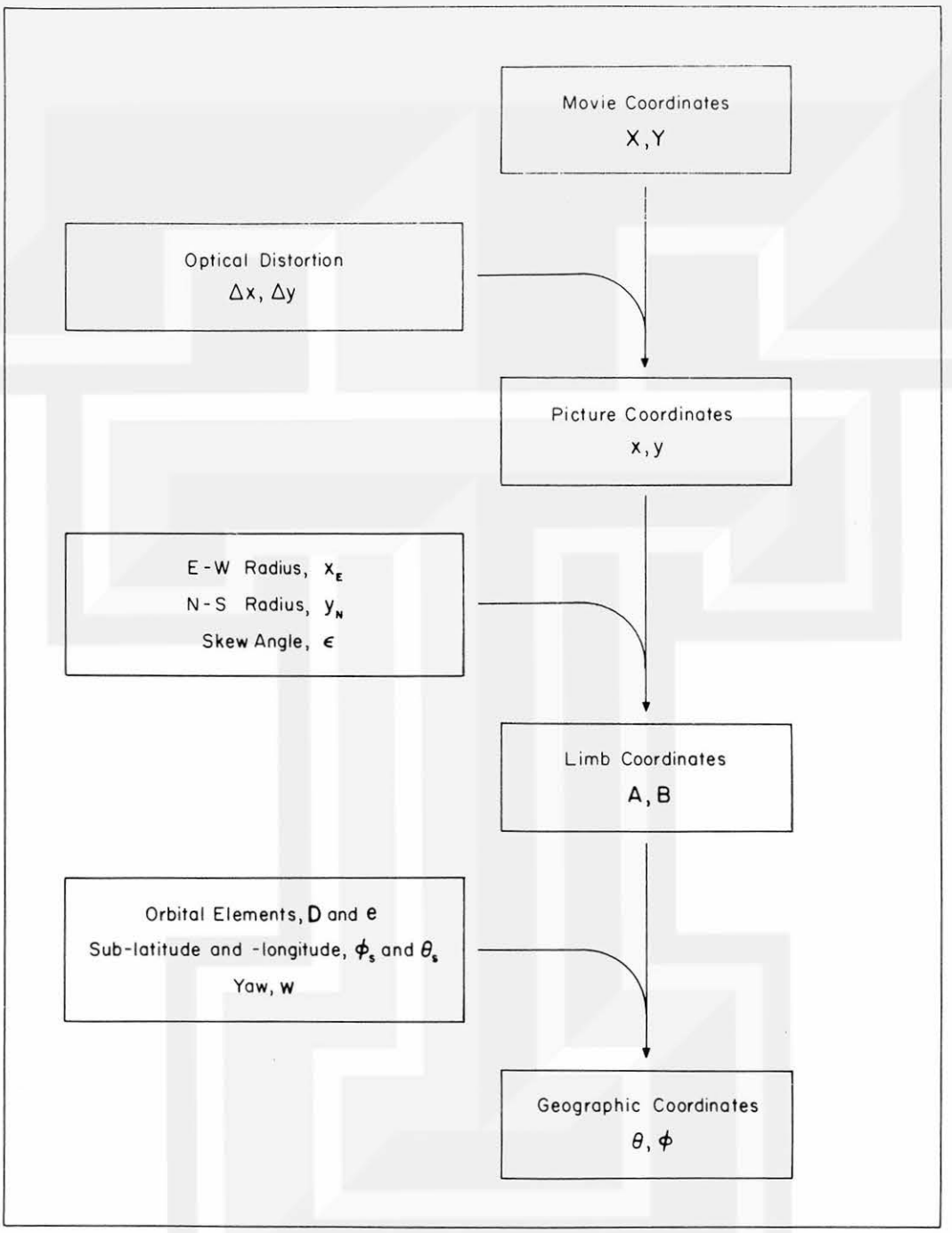

Fig. 11. Flow chart of coordinate transformations.

time interval it travels through this distance. Any looping motion of the cloud element between the beginning and end point is not considered.

If the arc length between the beginning and end points of a cloud vector is L: ϕ_1, ϕ_2 ; θ_1, θ_2 are the latitude and longitude of the beginning and end points, respectively, then

$$\cos L = \sin\phi_1 \sin\phi_2 + \cos\phi_1 \cos\phi_2 \cos(\theta_2 - \theta_1) \tag{11}$$

The speed of the cloud will be

$$V = \frac{aL}{\Delta t} \tag{12}$$

if we neglect the height of the cloud in comparison with the mean earth radius, a . Δt is the time interval between the beginning and end frames.

If Φ is the azimuth of the cloud vector, then (see Fig. 12)

$$\sin\phi_2 = \sin\phi_1 \cos L + \cos(\Phi) \cos\phi_1 \sin L \tag{13}$$

so that,

$$\Phi = \cos^{-1}\left(\frac{\sin\phi_2 - \sin\phi_1 \cos L}{\cos\phi_1 \sin L}\right) \tag{14}$$

Thus, the cloud velocity is determined.

8. EXAMPLE OF APPLICATION OF METRACOM TECHNIQUE

The METRACOM system was applied to determine the cloud velocities surrounding Hurricane Ginger during periods of approximately one hour during the four days from 25 through 28 September 1971 from the series of photographs taken by ATS III.

Motion of all elements that persisted during the time interval under study were traced as much as reasonable judgment allowed. The bright clouds, especially the cloud clusters that showed up distinctly as small spots were, by their appearance and configuration as well as their apparent flow pattern around the area surrounding the hurricane, attributed to be low clouds. They were the easiest tracked. On the other hand, those clouds that were fuzzy in appearance and extended over large areas were characteristic of high and/or middle clouds. Those within the area immediately surrounding the hurricane exhibited outflow motion. Flow pattern recognition through prior information from other sources regarding the general direction and relative speed of wind flow at high-cloud levels is a worthwhile guide in following the fuzzy-appearing clouds located some distance from the cyclone circulation. Tracking these elements posed difficulties

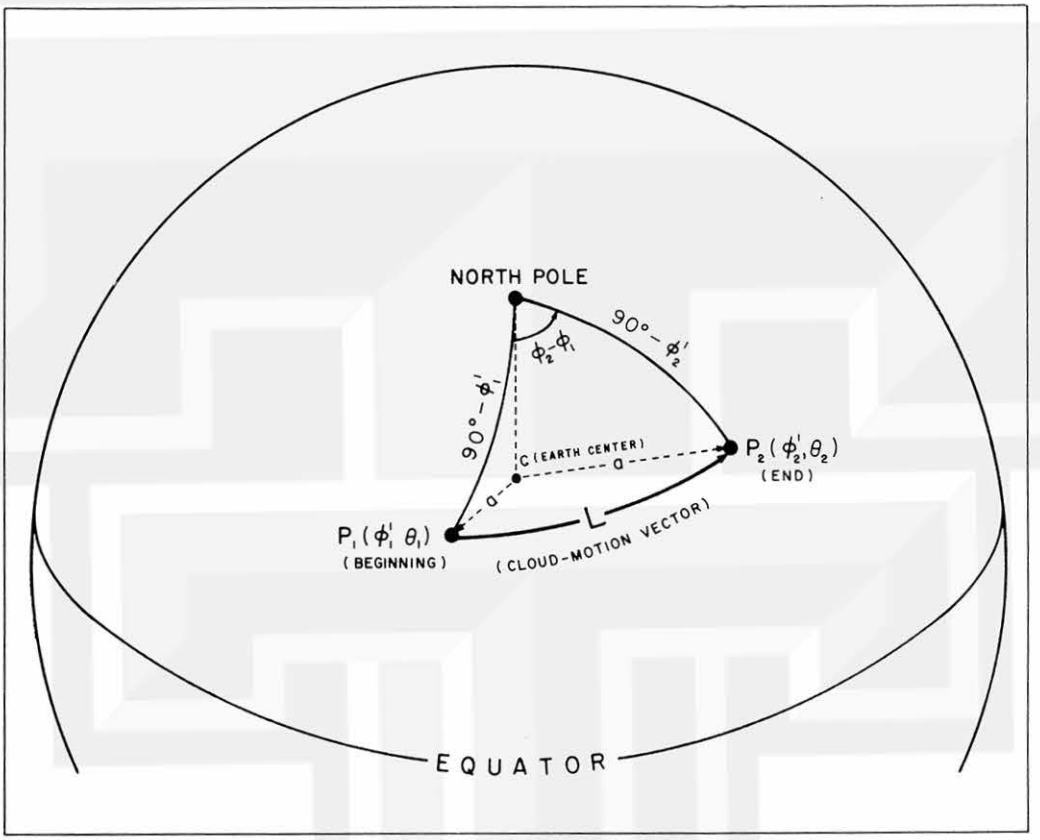

Fig. 12. The projection of cloud velocity vector $\overrightarrow{P_1 P_2}$ (heavy arrow) on the earth, where C is the earth center. $P_1(\phi_1', \theta_1)$, $P_2(\phi_2', \theta_2)$ are the beginning and end points of the vector $\overrightarrow{P_1 P_2}$, respectively, and a is the mean earth radius.

and was done with extreme care. Where distinction and tracing of cloud elements within the areas of large and uniform-intensity clouds were not clearly defined, following the movement of the edges of clouds that preserve their form was resorted to. In addition to the cloud elements, holes in clouds were also tracked for as long as their configuration and size remained constant. Recognizing middle clouds in themselves cannot yet be done with confidence unless they were known to exist beforehand.

As an illustration, cloud velocity vectors for a one-hour period on 25 September 1971 around Hurricane Ginger (see Fig. 13) were computed. The cloud flow patterns are shown in two different levels. The level assumed representative of the low-cloud flow was the surface (Fig. 14). Here the cloud vectors were plotted together with a number of surface synoptic observations for the synoptic hour (1200 Z) nearest the computation

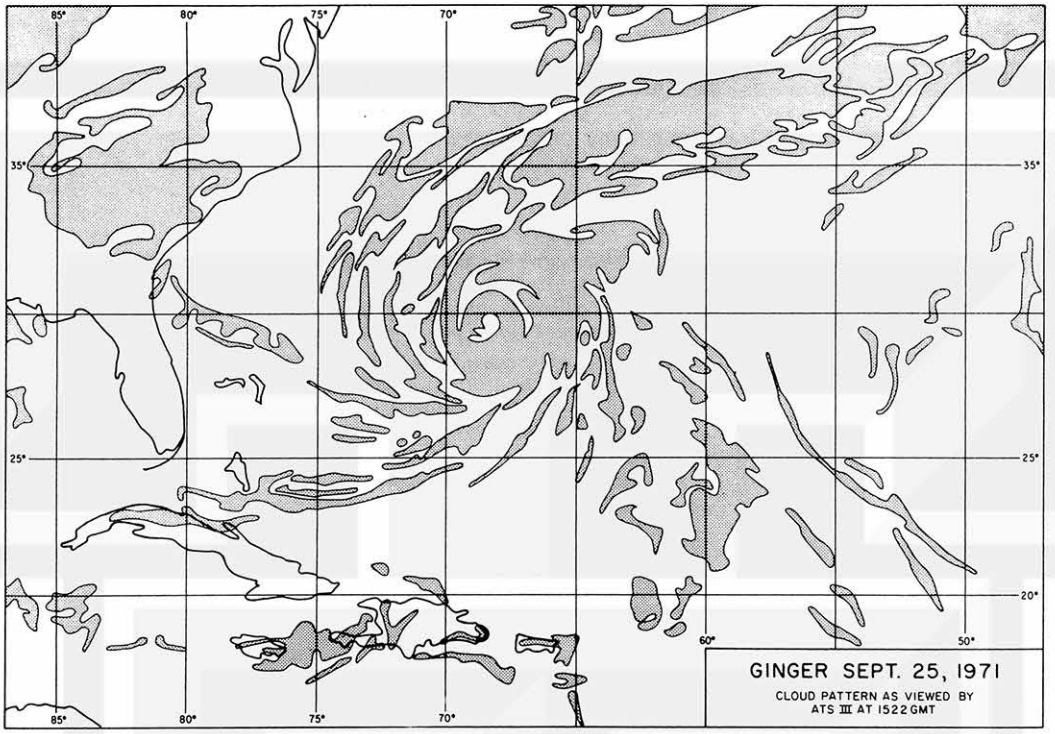

Fig. 13. Cloud patterns surrounding Hurricane Ginger and adjacent areas on September 25, 1971 at 1522 GMT, the beginning time at which cloud velocities were computed.

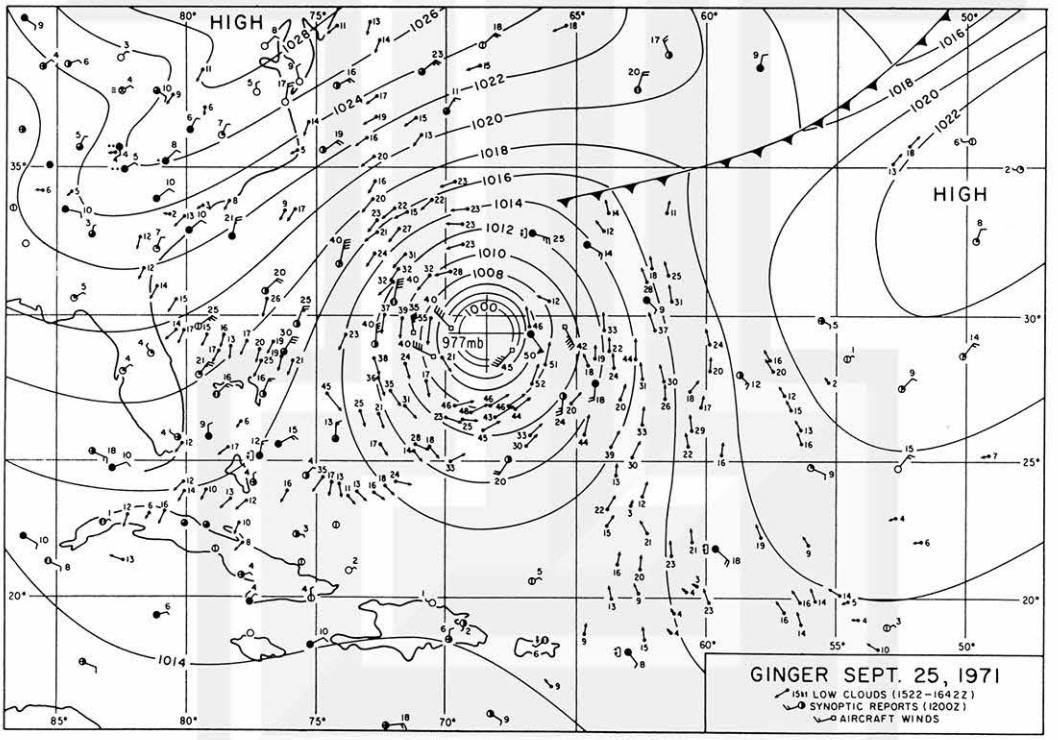

Fig. 14. Computed velocities and patterns of low cloud motion for area shown in Fig. 13 for cloud displacements during the period between 1522 and 1642 GMT. Surface isobaric analysis is superimposed together with a few surface synoptic observations for the nearest synoptic hour (1200 GMT) and relevant aircraft wind reports are included.

period and a few aircraft wind reports against a background of surface isobaric analysis. For the middle and high clouds, the level chosen was 200 mbs. On this streamline analysis chart (Fig. 15) the cloud vectors were plotted together with the observed upper winds also for the 1200 Z synoptic hour and with a few aircraft winds.

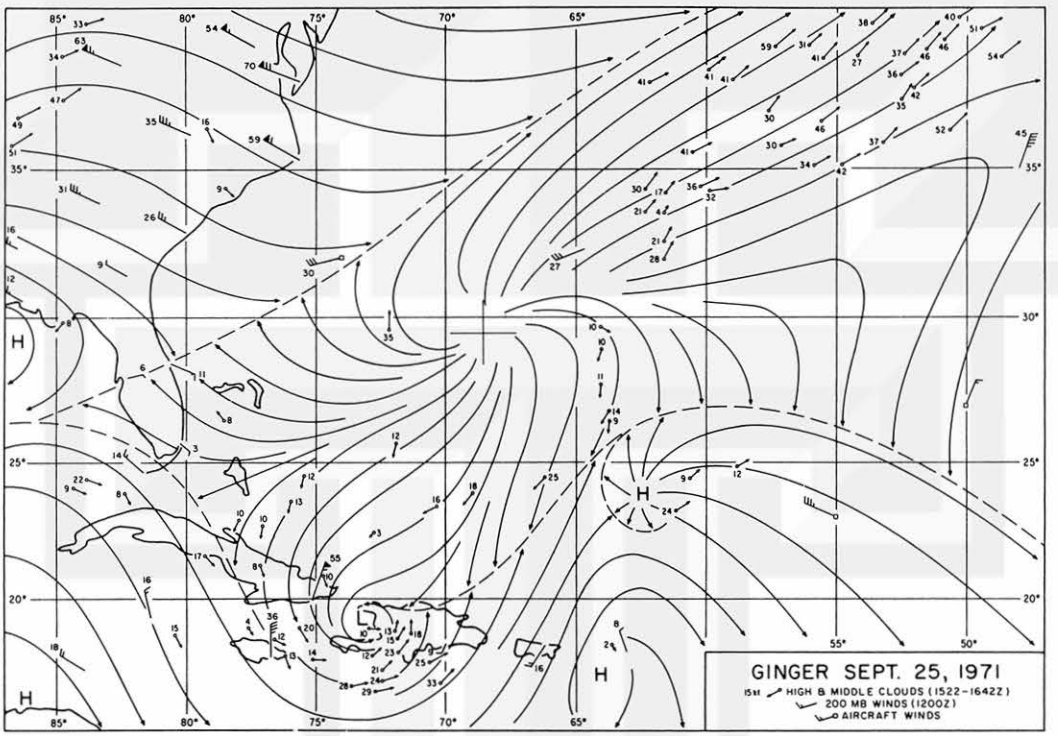

Fig. 15. Computed velocities and patterns of high and/or middle cloud motion for area shown in Fig. 13 during the same period indicated in Fig. 14 Streamline analysis is superimposed together with available upper wind observations at 200 mbs for the nearest synoptic hour (1200 GMT) and relevant aircraft wind reports are included.

The scarcity of computed vectors in the immediate vicinity of the eye of the hurricane, in the broad area streaming outward northeast of the eye and over the eastern mainland of the United States is noticeable. This arose from the lack of distinct elements that could be tracked in spite of the fact that the general direction of flow could be easily observed.

REFERENCES

Fujita, T. T. 1969: Present Status of Cloud Velocity Computations from the ATS I and ATS III Satellites. COSPAR Space Research Paper IX, Proceedings of Open Meetings of Working Groups of the Eleventh Plenary Meeting of COSPAR. Tokyo, 9-21 May 1968, pp 557-570.

_____, D. L. Bradbury, C. Murino, and L. Hull, 1968: A Study of Mesoscale Cloud Motions Computed from ATS-I and Terrestrial Photographs. SMRP Research Paper 71, University of Chicago, 25 pp.

Serebreny, S., W. E. Evans, R. G. Hadfield, and E. J. Wiegman, 1967: Detection of Cloud Displacement Using Video Techniques. Stanford Research Institute, Menlo Park, California, 37 pp.

Suomi, V. E., et al., 1972: McIDAS, Man-Computer Interaction Data Access System. Space Science and Engineering Center, University of Wisconsin-Madison, 39 pp.

APPENDIX A

Symbols and Notations

Greek Symbols

α Azimuth. Horizontal direction expressed in degrees measured clockwise from an adopted reference direction, usually true north.

δ Subpoint distance in geocentric angle.

ϵ Skew angle of the image.

η Nadir angle. The angle measured at the satellite between the line from the satellite to the center of the earth and the line from the satellite to a reference point.

η_{MAX} Maximum nadir angle. The maximum angle at the satellite between the line from the satellite to a reference point.

ϕ' Geocentric latitude of a point.

ϕ'_s Geocentric latitude of the satellite.

ϕ_s Subsatellite latitude.

θ_s Subsatellite longitude.

Roman Symbols

a Mean radius of the earth.

A_E East-west radius of the limb (or earth image) in Limb Grid unit.

B_N North-south radius of the limb (or earth image) in Limb Grid unit.

D Geocentric distance of the satellite.

D_E East-west diameter of the earth image.

e Eccentricity of the ~~orbit of the satellite.~~ earth

k Proportionality constant.

w Yaw of the satellite. The angle from true north clockwise to the projection of the satellite spin axis (point up) at the subsatellite point.

x_E East-west radius of the earth image on the photograph in picture grid unit.

y_N The projection of north-south radius of the earth image on the y-axis in picture grid unit.

x_F Fiducial distance. The distance between the outer edges of the two upper reference fiducial line segments on the photograph.

x, y Picture coordinates on the Cartesian Grid or rectangular coordinate system.

A, B Limb coordinates on the Limb Grid.

x_I, y_I Picture coordinates of the identified landmark on the local enlargement pictures.

F_x, F_y Scale factors between the global picture and the local enlargement pictures in x and y directions respectively.

APPENDIX B

Determination of Geographic Coordinates (ϕ, θ) of Cloud Object from Picture Coordinates (x,y) Using Satellite Location (ϕ_s, θ_s) and Yaw (w) and Eccentricity (e) of Earth.

For any cloud object with Limb coordinate (A,B) as discussed in Section 3, its geographic coordinates, namely latitude (ϕ) and longitude (θ) can be determined by using certain spherical trigonometrical laws with known satellite parameters, namely subsatellite latitude, subsatellite longitude and yaw.

First, the azimuth (α) of the point P, which is the projection of a cloud object on the earth, is determined by

$$\alpha = w + \tan^{-1} \frac{A}{B} \qquad (B1)$$

where w is the yaw of the satellite (see Appendix C), and the Limb coordinates (A,B) of the object P can be obtained by knowing their picture coordinates (x,y) from the Cartesian Grid superposed on the photograph (Section 3). Then, from the plane triangle O'SP' in Fig. 16, where point O' is the center of the photograph, point P' is the projection of the object point P on the image, the nadir angle (η) of the satellite (S) can be expressed by

$$\tan \eta = \frac{\sqrt{A^2 + B^2}}{1000} \cdot \eta_{MAX} \qquad (B2)$$

where η_{MAX} is the maximum nadir angle which can be obtained from the following equation using Δ CSK in Fig. 16, where C is the earth center and K is the tangent point where a line passes through the satellite (S) tangent to the scan equator;

$$\eta_{MAX} = \sin^{-1} \left(\frac{a}{D} \right) \qquad (B3)$$

where D is the geocentric distance of the satellite.

From the plane triangle Δ CSP in Fig. 16, the sine law gives

$$\sin \frac{\left[\pi - (\delta + \eta) \right]}{D} = \frac{\sin \eta}{a} \qquad (B4)$$

where δ is the subpoint distance of the point P in geocentric angle. Therefore,

$$\delta = -\eta + \sin^{-1} \left(\frac{D}{a} \sin \eta \right) \qquad (B5)$$

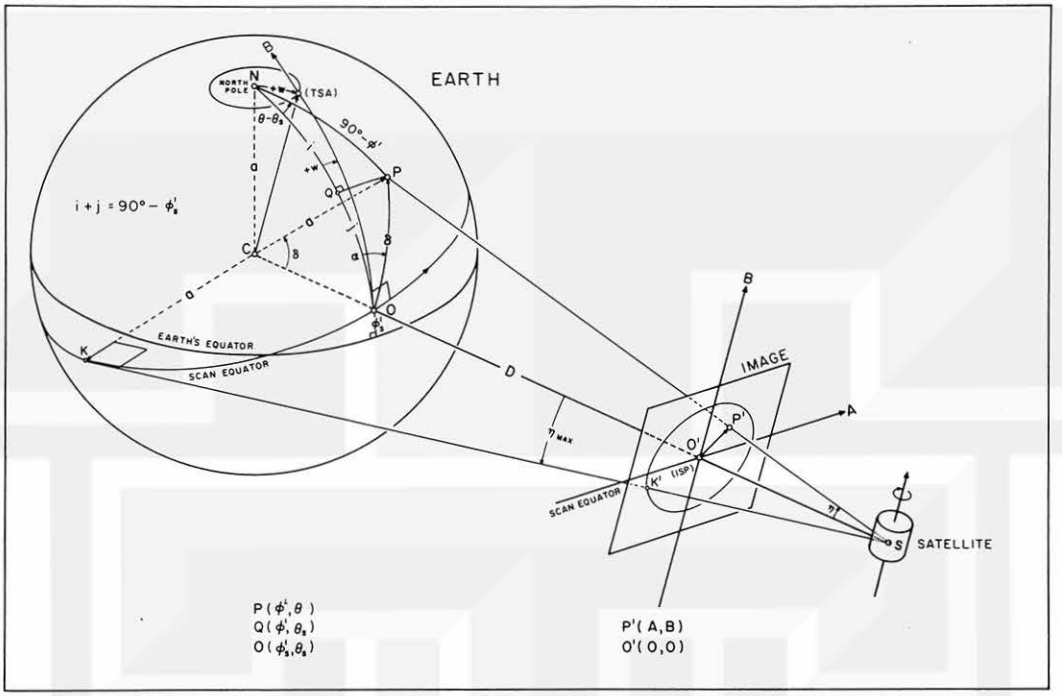

Fig. 16. Spherical geometry of the earth and its relative position to the earth image plane and the satellite (S). P is any point on the ground, O is the terrestrial subpoint (TSP). For variables, see Appendix A.

Then, for spherical triangle OPN in Fig. 16, and by the cosine law for sides,

$$\sin\phi' = \sin\phi'_s \cos\delta + \sin\delta \cos\phi'_s \cos\alpha \qquad (B6)$$

where ϕ' is the geocentric latitude of the point P and ϕ'_s is the geocentric latitude of the satellite. The latter is calculated by

$$\tan\phi'_s = (1 - e)\tan\phi_s$$

where the eccentricity is e ~~is the only input parameter used from NASA data~~ and ϕ_s is the subsatellite latitude which can be determined by using landmarks (see Appendix C).

The longitude of the point P can then be obtained by knowing ϕ' in the following equation (see spherical triangle OPN in Fig. 16)

$$\frac{\sin(\theta-\theta_s)}{\sin\delta} = \frac{\sin\alpha}{\sin(90°-\phi')} \qquad (B7)$$

where θ_s is the subsatellite longitude which can be determined by using landmark (see Appendix C).

Finally,

$$\tan \phi = (1 - e) \tan \phi' \qquad (B8)$$

Hence, the latitude (ϕ) and longitude (θ) of any cloud object P are

$$\theta = \theta_s + \sin^{-1} \left(\frac{\sin\delta \sin\alpha}{\cos\phi'} \right) \qquad (B9)$$

and

$$\phi = \tan^{-1} \left[(1 - e) \tan \phi' \right] \qquad (B10)$$

The flow chart for determining the latitude and longitude of any cloud object which has the projection point P on the earth is shown in Fig. 17.

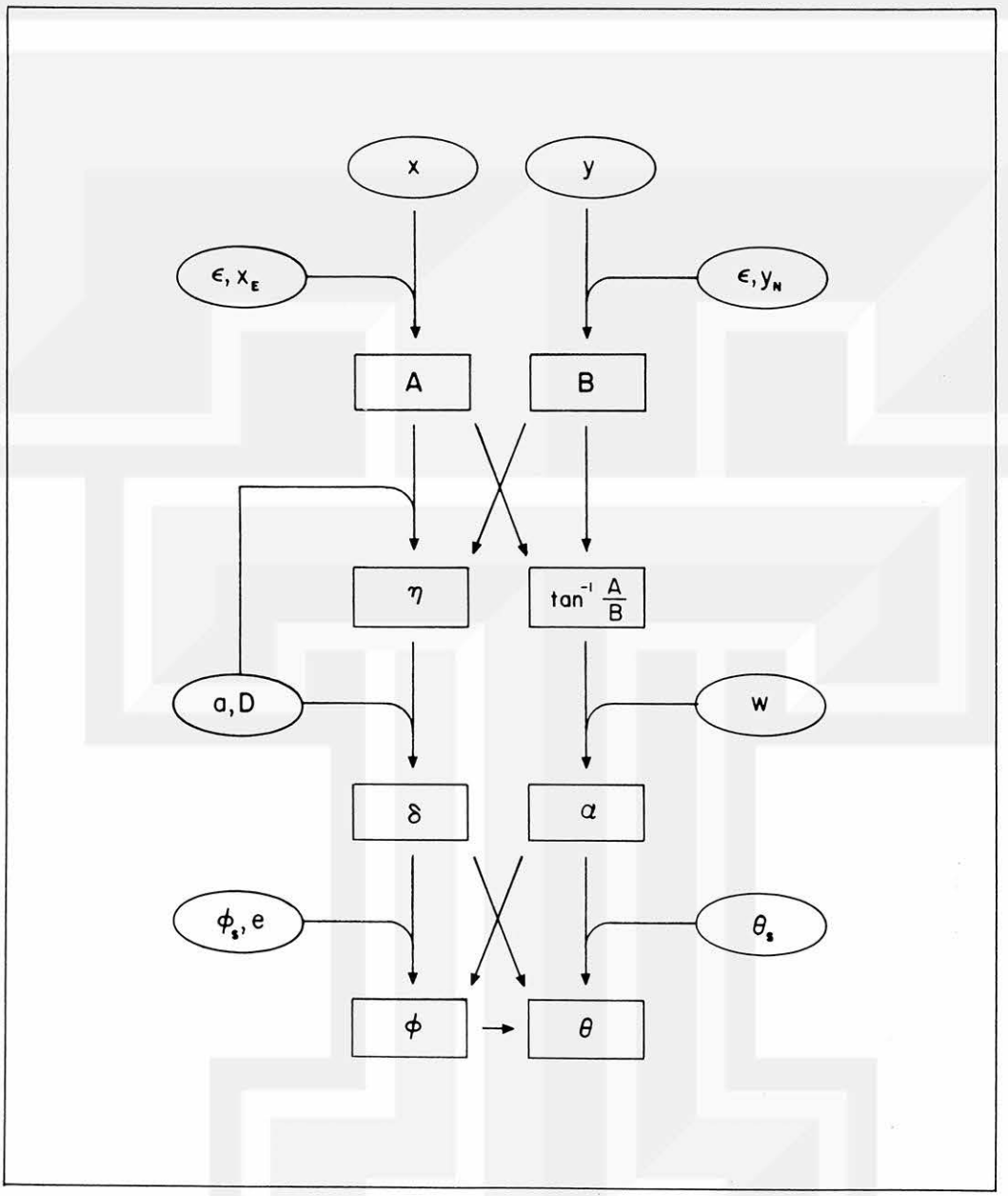

Legend : ⬭ input parameters

▭ computed variables

Note: ϕ = latitude of cloud object

θ = longitude of cloud object

$\tan^{-1}\frac{A}{B} = \alpha - w$

Fig. 17. Flow chart for the determination of geographical coordinates of cloud object.

APPENDIX C

Determination of Photogrammetric Parameters, Subsatellite Latitude (ϕ_s), Subsatellite Longitude (θ_s) and Yaw (w) by Using Known Landmarks and Eccentricity (e) of Earth.

A foil with all identifiable landmarks drawn and including the equator is attached on the global picture for the beginning and end frames by aligning them based on the best fit of all landmarks. Yaw (w) is thus obtained as the angle between the earth's equator and the scan line at or near equator. The latitude and longitude of the center point of the picture is the first guess of subsatellite latitude, ϕ_s , and subsatellite longitude, θ_s . By knowing ϕ_s , θ_s , and w , the latitude and longitude of any identified landmark on the photograph can be calculated (see Appendix B with landmark as the object point p). Variations of ϕ_s and θ_s from the first guess will also vary the calculated latitude and longitude of the landmark. It is found that the variation is approximately linear. Therefore, in order to reduce the error of the subsatellite point position to minimum, the subsatellite latitude and longitude is determined as that which gives the exact latitude and longitude of the landmark.

As an example, for this study of Hurricane Ginger on September 25, 1971 the determined parameters are listed in Table I.

TABLE I. Determined subsatellite latitude, subsatellite longitude and yaw for September 25, 1971.

Determined Parameters	Beginning Frame	End Frame
Subsatellite Latitude (°N)	+1.808	+1.794
Subsatellite Longitude (°W)	68.95	68.95
Yaw (°)	-0.773	-0.205

MESOMETEOROLOGY PROJECT - - - RESEARCH PAPERS

(Continued from front cover)

42.* A Study of Factors Contributing to Dissipation of Energy in a Developing Cumulonimbus - Rodger A. Brown and Tetsuya Fujita

43. A Program for Computer Gridding of Satellite Photographs for Mesoscale Research - William D. Bonner

44. Comparison of Grassland Surface Temperatures Measured by TIROS VII and Airborne Radiometers under Clear Sky and Cirriform Cloud Conditions - Ronald M. Reap

45. Death Valley Temperature Analysis Utilizing Nimbus I Infrared Data and Ground-Based Measurements - Ronald M. Reap and Tetsuya Fujita

46. On the "Thunderstorm-High Controversy" - Rodger A. Brown

47. Application of Precise Fujita Method on Nimbus I Photo Gridding - Lt. Cmd. Ruben Nasta

48. A Proposed Method of Estimating Cloud-top Temperature, Cloud Cover, and Emissivity and Whiteness of Clouds from Short- and Long-wave Radiation Data Obtained by TIROS Scanning Radiometers - T. Fujita and H. Grandoso

49. Aerial Survey of the Palm Sunday Tornadoes of April 11, 1965 - Tetsuya Fujita

50. Early Stage of Tornado Development as Revealed by Satellite Photographs - Tetsuya Fujita

51. Features and Motions of Radar Echoes on Palm Sunday, 1965 - D. L. Bradbury and T. Fujita

52. Stability and Differential Advection Associated with Tornado Development - Tetsuya Fujita and Dorothy L. Bradbury

53. Estimated Wind Speeds of the Palm Sunday Tornadoes - Tetsuya Fujita

54. On the Determination of Exchange Coefficients: Part II - Rotating and Nonrotating Convective Currents - Rodger A. Brown

55. Satellite Meteorological Study of Evaporation and Cloud Formation over the Western Pacific under the Influence of the Winter Monsoon - K. Tsuchiya and T. Fujita

56. A Proposed Mechanism of Snowstorm Mesojet over Japan under the Influence of the Winter Monsoon - T. Fujita and K. Tsuchiya

57. Some Effects of Lake Michigan upon Squall Lines and Summertime Convection - Walter A. Lyons

58. Angular Dependence of Reflection from Stratiform Clouds as Measured by TIROS IV Scanning Radiometers - A. Rabbe

59. Use of Wet-beam Doppler Winds in the Determination of the Vertical Velocity of Raindrops inside Hurricane Rainbands - T. Fujita, P. Black and A. Loesch

60. A Model of Typhoons Accompanied by Inner and Outer Rainbands - Tetsuya Fujita, Tatsuo Izawa,, Kazuo Watanabe and Ichiro Imai

61. Three-Dimensional Growth Characteristics of an Orographic Thunderstorm System - Rodger A. Brown

62. Split of a Thunderstorm into Anticyclonic and Cyclonic Storms and their Motion as Determined from Numerical Model Experiments - Tetsuya Fujita and Hector Grandoso

63. Preliminary Investigation of Peripheral Subsidence Associated with Hurricane Outflow - Ronald M. Reap

64. The Time Change of Cloud Features in Hurricane Anna, 1961, from the Easterly Wave Stage to Hurricane Dissipation - James E. Arnold

65. Easterly Wave Activity over Africa and in the Atlantic with a Note on the Intertropical Convergence Zone during Early July 1961 - James E. Arnold

66. Mesoscale Motions in Oceanic Stratus as Revealed by Satellite Data - Walter A. Lyons and Tetsuya Fujita

67. Mesoscale Aspects of Orographic Influences on Flow and Precipitation Patterns - Tetsuya Fujita

68. A Mesometeorological Study of a Subtropical Mesocyclone -Hidetoshi Arakawa, Kazuo Watanabe, Kiyoshi Tsuchiya and Tetsuya Fujita

69. Estimation of Tornado Wind Speed from Characteristic Ground Marks - Tetsuya Fujita, Dorothy L. Bradbury and Peter G. Black

70. Computation of Height and Velocity of Clouds from Dual, Whole-Sky, Time-Lapse Picture Sequences - Dorothy L. Bradbury and Tetsuya Fujita

71. A Study of Mesoscale Cloud Motions Computed from ATS-I and Terrestrial Photographs - Tetsuya Fujita, Dorothy L. Bradbury, Clifford Murino and Louis Hull

72. Aerial Measurement of Radiation Temperatures over Mt. Fuji and Tokyo Areas and Their Application to the Determination of Ground- and Water-Surface Temperatures - Tetsuya Fujita, Gisela Baralt and Kiyoshi Tsuchiya

73. Angular Dependence of Reflected Solar Radiation from Sahara Measured by TIROS VII in a Torquing Maneuver - Rene Mendez.

74. The Control of Summertime Cumuli and Thunderstorms by Lake Michigan During Non-Lake Breeze Conditions - Walter A. Lyons and John W. Wilson

75. Heavy Snow in the Chicago Area as Revealed by Satellite Pictures - James Bunting and Donna Lamb

76. A Model of Typhoons with Outflow and Subsidence Layers - Tatsuo Izawa

* out of print

(continued on outside back cover)

SATELLITE AND MESOMETEOROLOGY RESEARCH PROJECT --- PAPERS
(Continued from inside back cover)

77. Yaw Corrections for Accurate Gridding of Nimbus HRIR Data - Roland A. Madden

78. Formation and Structure of Equatorial Anticyclones Caused by Large-Scale Cross Equatorial Flows Determined by ATS I Photographs - Tetsuya T. Fujita and Kazuo Watanabe and Tatsuo Izawa.

79. Determination of Mass Outflow from a Thunderstorm Complex Using ATS III Pictures - T. T. Fujita and D. L. Bradbury.

80. Development of a Dry Line as Shown by ATS Cloud Photography and Verified by Radar and Conventional Aerological Data - Dorothy L. Bradbury.

81. Dynamical Analysis of Outflow from Tornado-Producing Thunderstorms as Revealed by ATS III Pictures - K. Ninomiya.

82.** Computation of Cloud Heights from Shadow Positions through Single Image Photogrammetry of Apollo Pictures - T. T. Fujita.

83. Aircraft, Spacecraft, Satellite and Radar Observations of Hurricane Gladys, 1968 - R. Cecil Gentry, Tetsuya T. Fujita and Robert C. Sheets.

84. Basic Problems on Cloud Identification Related to the Design of SMS-GOES Spin Scan Radiometers - Tetsuya T. Fujita.

85. Mesoscale Modification of Synoptic Situations over the Area of Thunderstorms' Development as Revealed by ATS III and Aerological Data - K. Ninomiya.

86. Palm Sunday Tornadoes of April 11, 1965 - T. T. Fujita, Dorothy L. Bradbury and C. F. Van Thullenar (Reprint from Mon. Wea. Rev., 98, 29-69, 1970).

87. Patterns of Equivalent Blackbody Temperature and Reflectance of Model Clouds Computed by Changing Radiometer's Field of View - Jaime J. Tecson.

88. Lubbock Tornadoes of 11 May 1970 - Tetsuya Theodore Fujita.

89. Estimate of Areal Probability of Tornadoes from Inflationary Reporting of Their Frequencies - Tetsuya T. Fujita.

90. Application of ATS III Photographs for Determination of Dust and Cloud Velocities Over Northern Tropical Atlantic - Tetsuya T. Fujita.

91. A Proposed Characterization of Tornadoes and Hurricanes by Area and Intensity - Tetsuya T. Fujita.

92. Estimate of Maximum Wind Speeds of Tornadoes in Three Northwestern States - T. Theodore Fujita.

93. In- and Outflow Field of Hurricane Debbie as Revealed by Echo and Cloud Velocities from Airborne Radar and ATS-III Pictures - T. T. Fujita and P. G. Black (Reprinted from preprint of Radar Meteorology Conference, November 17-20, 1970, Tucson, Arizona).

94. Characterization of 1965 Tornadoes by their Area and Intensity - Jaime J. Tecson.

95.* Computation of Height and Velocity of Clouds over Barbados from a Whole-Sky Camera Network - Richard D. Lyons.

96. The Filling over Land of Hurricane Camille, August 17-18, 1969 - Dorothy L. Bradbury.

97. Tornado Occurrences Related to Overshooting Cloud-Top Heights as Determined from ATS Pictures - T. Theodore Fujita.

98.** F P P Tornado Scale and its Applications - T. Theodore Fujita and A. D. Pearson.

99. Preliminary Results of Tornado Watch Experiment 1971 - T. T. Fujita, J. J. Tecson and L. A. Schaal.

100. F-Scale Classification of 1971 Tornadoes - T. Theodore Fujita.

101. Typhoon-Associated Tornadoes in Japan and New Evidence of Suction Vortices in a Tornado near Tokyo - T. Theodore Fujita.

102. Proposed Mechanism of Suction Spots Accompanied by Tornadoes - T. Theodore Fujita.

103. A Climatological Study of Cloud Formation over the Atlantic During Winter Monsoon - H. Shitara

104.** Statistical Analysis of 1971 Tornadoes - Edward W. Pearl

105. Estimate of Maximum Windspeeds of Tornadoes in Southernmost Rockies - T. Theodore Fujita.

106. Use of ATS Pictures in Hurricane Modification - T. Theodore Fujita.

107. Mesoscale Analysis of Tropical Latin America - T. Theodore Fujita.

108. Tornadoes Around The World - T. Theodore Fujita. (Reprinted from Weatherwise, Vol 26, No. 2, April 1973)

109. A Study of Satellite-Observed Cloud Patterns of Tropical Cyclones - Ekundayo E. Balogun.